ELSEVIER

Cement & Concrete Composites 24 (2002) 347–350

Cement & Concrete Composites

www.elsevier.com/locate/cemconcomp

Identification of thaumasite in concrete by Raman chemical imaging

Sadananda Sahu [a,*], David L. Exline [b], Matthew P. Nelson [b]

[a] R.J. Lee Group Inc., 350 Hochberg Road, Monroeville, PA 15146, USA
[b] ChemIcon Inc., 7301 Penn Avenue, Pittsburgh, PA 15208, USA

Abstract

Identification of thaumasite ($CaSiO_3 \cdot CaO_3 \cdot CaSO_4 \cdot 15H_2O$) in concrete undergoing external sulfate attack by X-ray powder diffraction or by microscopic techniques is difficult due to its crystallographic and morphological similarity with ettringite. Widefield Raman chemical imaging via liquid crystal tunable filter (LCTF) technology has been used in a preliminary study to determine the presence of thaumasite in association with ettringite ($3CaO \cdot Al_2O_3 \cdot 3CaSO_4 \cdot 32H_2O$) and gypsum ($CaSO_4 \cdot 2H_2O$). Raman chemical imaging combines Raman spectroscopy with optical microscopy and digital imaging to provide images with molecular-based contrast. Thaumasite has three major peaks at 658, 990, 1076 cm^{-1} and three minor peaks at 417, 453, 479 cm^{-1}. Ettringite has major peaks at 990, 1088 cm^{-1}. Gypsum has a major peak at 1009 cm^{-1} and minor peaks at 417, 496, 621, 673, 1137 cm^{-1}. When these minerals are presented together, Raman chemical imaging provides an excellent way to determine their molecular composition and spatial distribution within the sample.

Keywords: Raman chemical imaging; Thaumasite; Ettringite; Gypsum; LCTF

1. Introduction

Formation of ettringite and gypsum as deleterious products during the external sulfate attack of concrete is well recognized [1]. Formation of these minerals in a hardened concrete leads to expansion and cracking. Several recent studies report that during sulfate attack a third mineral, thaumasite forms in the system in conjunction with gypsum and ettringite [2–9]. Thaumasite formation by sulfate attack is recognized to be detrimental to concrete durability because its formation consumes the binder phase, C–S–H [1]. Thaumasite forms when carbonate containing rocks/fillers are present in a concrete exposed to sulfate ions in ground water at low temperatures (5–10 °C) [2,3]. A recent study shows that thaumasite can also form in concrete without any carbonate containing aggregates [9]. The required carbonate ions for the formation of thaumasite are derived from external sources when concrete is exposed to the atmosphere or ground water for extended periods.

Identification of thaumasite is difficult using X-ray diffraction (XRD) and optical microscopy due to its similarity in crystallographic structure and morphology to ettringite. Scanning electron microscope (SEM) coupled with X-ray energy dispersive spectroscopy (EDS) is useful for identifying the elemental content of thaumasite and ettringite in concrete. Ettringite has three distinct peaks of Al, S, Ca while thaumasite has the distinct peaks of Si, Al, Ca. The carbon peak of thaumasite is not easy to detect by EDS.

Raman spectroscopy is another technique that has been used in identifying thaumasite [10–12]. This technique has an advantage in identifying thaumasite as it has a distinct peak at 658 cm^{-1} corresponding to Si [6]. In a recent study, Raman microprobe spectroscopy was used to distinguish thaumasite from ettringite in deteriorated concrete [12].

The recent development of Raman chemical imaging [13–19], which combines the molecular analysis capabilities of Raman spectroscopy and the visualization power of an optical microscope, provides a potential solution for obtaining molecular information on various minerals of concrete. Raman chemical imaging is based on Raman spectroscopy, which reveals the molecular composition of materials. Raman chemical imaging utilizes wide field illumination and liquid crystal tunable filters (LCTFs) to provide images with molecular-based contrast. The spectral resolving power of the LCTF is

* Corresponding author. Tel.: +1-724-325-1776; fax: +1-724-733-1799.
E-mail address: ssahu@rjlg.com (S. Sahu).

0958-9465/02/$ - see front matter
PII: S0958-9465(01)00086-5

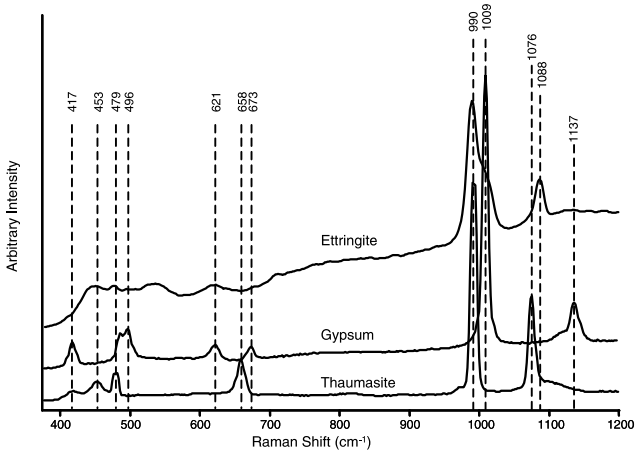

Fig. 1. Overlaid spectra of thaumasite, ettringite and gypsum (532 nm laser excitation, 10× magnification, 5 s acquisition).

high due to the narrow band pass (<9 cm^{-1}). LCTF Raman microscopy provides diffraction-limited spatial resolution of 250 nm with appropriate high numerical aperture microscope objectives. Although relatively new, Raman chemical imaging is a proven molecular imaging technology.

In the present investigation, Raman chemical imaging is used to identify the spatial distribution of thaumasite in association with ettringite and gypsum. In this study, only standard samples were used to simulate the environmental condition of thaumasite in a concrete.

2. Methodology

2.1. Materials

A sample of thaumasite was obtained from Ward's Natural Sciences. Its purity was checked by XRD and SEM–EDS. Ettringite was prepared in the R.J. Lee Group laboratory by mixing solutions of calcium hydroxide and aluminum sulfate. The phase purity was checked by XRD. Reagent grade gypsum was used as a standard.

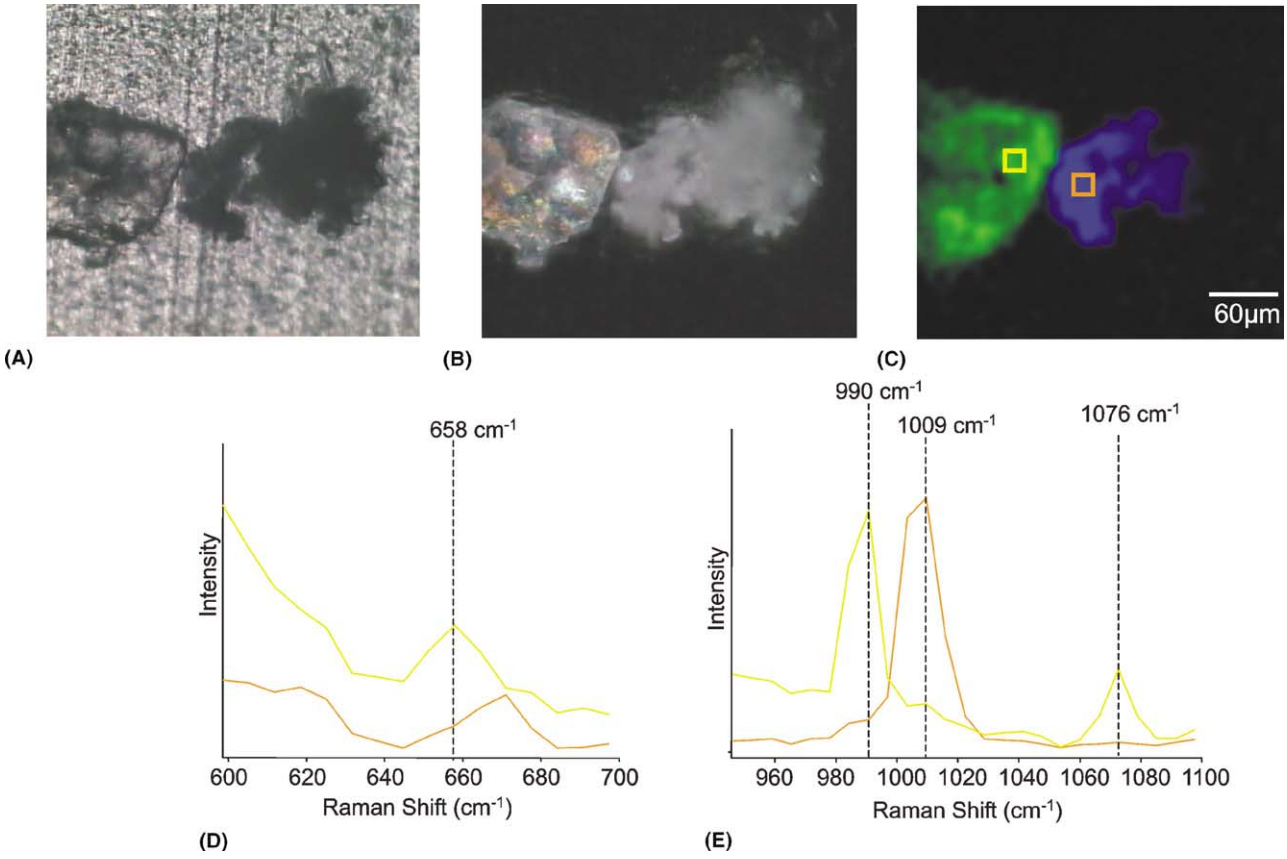

Fig. 2. Raman chemical imaging of thaumasite and gypsum: (A) Brightfield reflectance image; (B) polarized light image; (C) RGB image; and (D) LCTF-generated Raman spectra associated with thaumasite (yellow box) and gypsum (orange box), respectively. (10× magnification, 20 s per frame, LCTF tuning parameters: 600–700 and 950–1100 cm^{-1}, 17 W/cm^2 laser power density at sample).

2.2. Optical microscopy, Raman spectroscopy and chemical imaging analysis

A FALCON™ Raman Chemical Imaging System (ChemIcon, Pittsburgh, PA) equipped with 532 nm laser excitation and a 100 W quartz tungsten halogen (QTH) broad band source was used to collect brightfield microscopic images, Raman chemical images and dispersive Raman spectra. Acquisition Manager 5.0 (ChemIcon) and Chemimage 5.0 (ChemIcon) software packages were used for data acquisition, analysis and visualization. Raman chemical imaging data were generated by tuning the LCTF from 600–700 and 950–1100 cm^{-1} in 7 cm^{-1} increments.

2.3. Sample preparation

Known samples of thaumasite, ettringite and gypsum were prepared by placing a small amount of material on a glass microscope slide and mixing them together. Samples were isolated by manual optical microscopy (10× magnification) and Raman dispersive spectra and Raman chemical images were acquired.

3. Results and discussion

The overlaid dispersive Raman spectra for all three samples are shown in Fig. 1. Ettringite has two major peaks at 990 and 1088 cm^{-1}, respectively. Gypsum has a major peak at 1009 and five minor peaks at 417, 496, 621, 673, and 1137 cm^{-1}, respectively. Thaumasite has three major peaks at 658, 990, and 1076 cm^{-1} corresponding to Si [6], sulfate and carbonate groups, respectively. There are also three minor peaks at 417, 453, and 479 cm^{-1} observed. The sulfate peaks for ettringite and thaumasite have similar Raman shift values making it difficult to distinguish between these two minerals based on these peaks alone. However, thaumasite has two distinct peaks at 658 and 1076 cm^{-1} corresponding to Si [6] and carbonate group, respectively. Thaumasite also has three unique minor peaks. Gypsum has a major peak at 1009 cm^{-1} and minor peaks at 417, 496, 621, 673, 1137 cm^{-1}, respectively. The peak positions of gypsum are different from thaumasite and ettringite, making it easier to distinguish gypsum in the presence of ettringite and/or thaumasite. Raman spectroscopy alone is a valuable tool to positively identify thaumasite in a

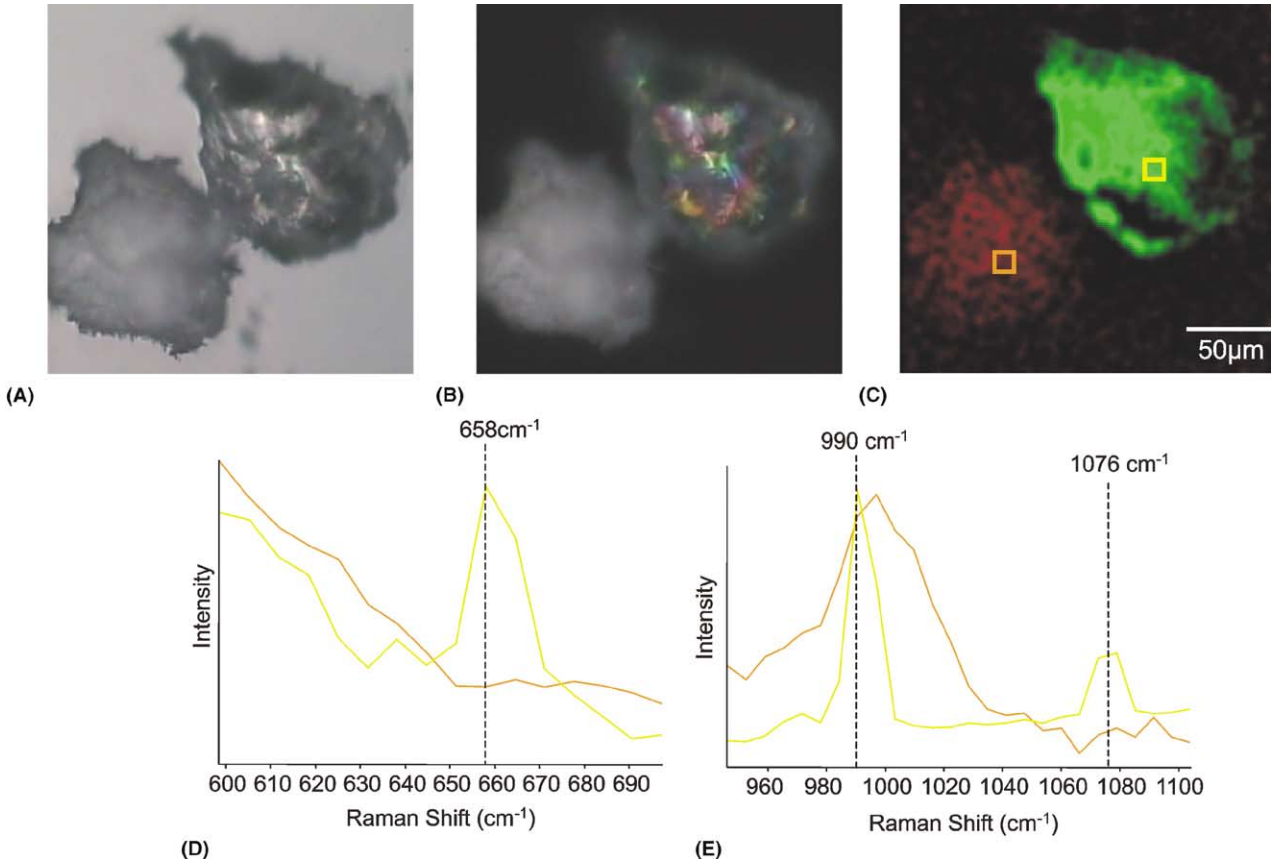

Fig. 3. Raman chemical imaging of thaumasite and ettringite: (A) Brightfield reflectance image; (B) polarized light image; (C) RGB image; and (D) LCTF-generated Raman spectra associated with thaumasite (yellow box) and ettringite (orange box), respectively. (10× magnification, 10 s per frame, LCTF tuning parameters: 600–700 and 950–1100 cm^{-1}, 43 W/cm^2 laser power density at sample).

mixture with ettringite and gypsum. However, it provides virtually no information about the spatial distribution of the minerals.

A brightfield reflectance and polarized light image of thaumasite and gypsum deposited on a glass microscope slide are shown in Figs. 2(A) and (B), respectively. Fig. 2(C) is a color composite Raman chemical image in which data associated with the thaumasite and gypsum particles have been assigned to the green and blue color channels, respectively. Figs. 2(D) and (E) show LCTF-generated Raman spectra associated with thaumasite (yellow box) and gypsum (orange box) in the 600–700 and 950–1100 cm^{-1} spectral regions, respectively. The LCTF spectra show the characteristic thaumasite peaks at 658 and 1076 cm^{-1}, respectively. The main peak of thaumasite is clearly separated from gypsum. Thaumasite is differentiated from gypsum in the polarized light image (Fig. 2(B)) due to its high birefringence relative to gypsum.

A brightfield reflectance and polarized light image of thaumasite and ettringite deposited on a glass microscope slide are shown in Figs. 3(A) and (B), respectively. Fig. 3(C) is a color composite Raman chemical image in which data associated with the thaumasite and ettringite particles have been assigned to the green and red color channels, respectively. Figs. 3(D) and (E) show LCTF-generated Raman spectra associated with thaumasite (yellow box) and ettringite (orange box) in the 600–700 and 950–1100 cm^{-1} spectral regions, respectively. The LCTF spectra show the characteristic thaumasite peak at 658 and 1076 cm^{-1}, respectively. There are no peaks in this spectral region for ettringite. The main peak of thaumasite and ettringite nearly overlap. Despite the similarities in peak positions, thaumasite and ettringite could be distinguished based on differences in spectral shapes (i.e. peak widths). Thaumasite is differentiated from ettringite in the polarized light image (Fig. 3(B)) due to its high birefringence relative to ettringite.

4. Conclusions

Raman dispersive spectroscopy is a useful technique to discriminate thaumasite in association with ettringite and gypsum. However, Raman dispersive spectroscopy alone does not provide information relative to the spatial distribution of the minerals. Raman chemical imaging analysis is shown here to be a powerful tool for mapping the spatial distribution of external sulfate attack products such as thaumasite, ettringite and gypsum in concrete. This preliminary study demonstrates the potential value of Raman chemical imaging in concrete analysis.

References

[1] Mehta PK. In: Concrete microstructure, properties and materials. 2nd ed. New York: McGraw-Hill; 1993. p. 146–8.
[2] Crammond NJ, Halliwell MA. The thaumasite form of sulfate attack in concretes containing a source of carbonate ions – a microstructural overview. In: 2nd Symposium Advances in Concrete Tech. ACI SP-154; 1995. p. 357–80.
[3] Crammond NJ, Halliwell MA. Assessment of the conditions required for the thaumasite form of sulfate attack. In: Scrivner KL, Young JF, editors. Mechanisms of chemical degradation of cement-based systems. E & FN Spon; 1997. p. 193–200.
[4] Collepardi M. Degradation and restoration of masonry walls of historical buildings. Mater Struct 1990;23:81–102.
[5] Berra M, Baronio G. Thaumasite in deteriorated concretes in the presence of sulfates. Concrete Durability. ACI SP-100; 1987. p. 2073–89.
[6] Ludwig U, Meher S. Destruction of historical building by the formation of ettringite and thaumasite. In: Proceedings of the 8th International Congress on the Chemistry of Cement, Rio de Janeiro, vol. V. 1986. p. 181–8.
[7] Bickley JA, Hemmings RT, Hooton RD, Balinski J. Thaumasite related deterioration of concrete structures. ACI SP-144; 1994. p. 159–75.
[8] Sarkar SL, Little DN. Microstructural investigation of severe distress in a crushed concrete base. Cem Concr Res 1998; 28(3):401–10.
[9] Sahu S, Badger S, Thaulow N. Evidence of thaumasite formation in Southern California concrete (this issue).
[10] Bensted J, Varma SP. Studies of thaumasite – Part II. Silic Ind 1974;39:11–9.
[11] Yang R, Buenfeld NR. Microstructural identification of thaumasite in concrete by backscattered electron imaging at low vacuum. Cem Concr Res 2000;30:775–9.
[12] Brough AR, Atkinson A. Micro-Raman spectroscopy of thaumasite. Cem Concr Res 2001;31:421–4.
[13] Kline NJ, Treado PJ. Raman chemical imaging of breast tissue. J Raman Spectrosc 1997;28:119–24.
[14] Treado PJ. Chemical imaging reveals more than the microscope. Laser Focus World 1995;31:75–82.
[15] Morris HR. Liquid crystal tunable filter Raman chemical imaging. Appl Spectrosc 1996;50:805–11.
[16] Schaeberle MD, Treado PJ. Raman chemical imaging spectroscopy. Anal Chem 1999;71:175A–81A.
[17] Schoonover JR et al. Integration of elemental and molecular imaging to characterize heterogeneous inorganic materials. Appl Spectrosc 1998;52:1505–14.
[18] Nelson MP, Zugates CT, Treado PJ, Casuccio GS, Exline DL, Schlaegle SF. Combining Raman chemical imaging and scanning electron microscopy to characterize ambient fine particulate matter. Aerosol Sci Technol 2001;34:108–17.
[19] Available from: http://stargate.jpl.nasa.gov/lctf/.